

## Electrodeposition of PbTe thin films from acidic nitrate baths

Feng Xiao<sup>a</sup>, Bongyoung Yoo<sup>a</sup>, Margaret A. Ryan<sup>b</sup>, Kyu-Hwan Lee<sup>c</sup>, Nosang V. Myung<sup>a,\*</sup>

<sup>a</sup> Department of Chemical and Environmental Engineering and Center for Nanoscale Science and Engineering,  
University of California-Riverside, Riverside, CA 92521, USA

<sup>b</sup> Materials and Device Technology Group, Jet Propulsion Laboratory, California Institute of Technology, Pasadena, CA 91109, USA

<sup>c</sup> Electrochemical Processing Group, Korea Institute of Machinery & Materials, Changwon-Si, Kyungnam 641-010, South Korea

Received 7 October 2005; received in revised form 7 June 2006; accepted 7 June 2006

Available online 2 August 2006

### Abstract

Electrodeposition of PbTe thin films from an acidic nitric bath was systematically investigated to understand the kinetics and the effect of electrodeposition conditions on film composition, crystallographic structure, texture and grain size. The electroanalytical studies employed initially with a rotating disk electrode to investigate the kinetics associated with Te, Pb and PbTe electrodeposition. The results indicated that the PbTe thin films were obtained by the underpotential deposition (UPD) of Pb atoms onto the overpotentially deposited Te atoms on a substrate.

Based on these studies, PbTe thin films were potentiostatically electrodeposited using e-beam evaporated gold thin films on silicon substrate to investigate the effect of various deposition conditions on film composition and microstructure. The data indicated that the microstructure, composition and preferred film growth orientation of PbTe thin films strongly depended on the applied potential and electrolyte concentration. At  $-0.12$  V, the film was granular, dense, and preferentially oriented in the  $[1\ 0\ 0]$  direction. At potentials more negative than  $-0.15$  V, the film was dendritic and preferentially oriented in the  $[2\ 1\ 1]$  direction. A smooth, dense and crystalline film with nearly stoichiometric composition was obtained at  $-0.12$  V from a solution containing  $0.01$  M  $\text{HTeO}_2^+$ ,  $0.05$   $\text{Pb}^{2+}$  and  $1$  M  $\text{HNO}_3$ .

© 2006 Elsevier Ltd. All rights reserved.

**Keywords:** Lead telluride; Electrodeposition; Thermoelectrics; Photodetector

### 1. Introduction

Lead telluride (PbTe) makes a good candidate material for photodetectors in the mid- and far-infrared bands and mid-infrared quantum well laser diode because of high quantum efficiencies, low noise level at working temperature and ability to tune peak wavelength by adjusting alloy composition [1–6]. PbTe is also among the most efficient materials for thermoelectric power generation in the intermediate range of temperature (500–900 K) because of its high thermoelectric figure of the merit (ZT), a high melting point, good chemical stability, low vapor pressure and good chemical strength [7–10].

Various vacuum deposition techniques have been utilized to deposit PbTe thin films including molecular beam epitaxy (MBE) [11], magnetron sputtering [12], thermal evaporation [13] and pulsed laser deposition [14]. Compared to these meth-

ods, electrodeposition is a simple, cost-effective and fast deposition technique which also allows precise control of composition, crystallographic structure, texture and grain size. In addition, nanoengineered material such as superlattice thin films and one-dimensional nanowires can be readily electrodeposited by modifying electrodeposition conditions.

Unfortunately, only a few studies have been conducted on the electrodeposition of PbTe thin films. Beaunier et al. [15] investigated epitaxial electrodeposition of PbTe thin films on  $(1\ 1\ 1)$  InP single crystal substrate from an acidic nitric bath containing Cd ions. In their work, they focused on the effect of Cd ion on the morphology of PbTe films. When  $0.5$  M  $\text{Cd}(\text{NO}_3)_2$  was added to electrolytes, the film morphologies were altered from dendritic growth to homogenous dense growth. Saloniemi et al. [16] reported the electrodeposition of PbTe from alkaline solutions (pH of 9) with EDTA as a complexing agent. They observed that a smooth, dense, Te-rich PbTe thin film could be fabricated on Cu and indium tin oxide (ITO) substrates. X-ray diffraction patterns indicated PbTe thin film had  $(2\ 0\ 0)$  preferred crystal orientation.

\* Corresponding author.

E-mail address: [myung@enr.ucr.edu](mailto:myung@enr.ucr.edu) (N.V. Myung).

Even though these studies demonstrated the feasibility of electrodeposition of PbTe thin films, previous efforts lacked a systematic study necessary to understand the deposition mechanisms and the effect of electrodeposition conditions on film composition, crystallographic structure, texture and grain size. In this work, electrodeposition of PbTe thin films was systematically investigated to understand electrochemical reactions and to optimize deposition conditions to achieve high quality PbTe thin films.

## 2. Experimental

An acidic nitric electrolyte was prepared by first dissolving  $\text{TeO}_2$  (99.9995%; Alfa Aesar, Inc.) in concentrated nitric acid. Next,  $\text{Pb}(\text{NO}_3)_2$  was dissolved in a separate beaker. Once the solids were dissolved, they were mixed together and water was added to reach the final volume. The effect of tellurium ion concentration on the electrodeposition of PbTe was investigated in two different electrolytes (i.e. 0.01 M  $\text{HTeO}_2^+$  (high tellurium ion bath) and 0.0001 M  $\text{HTeO}_2^+$  (low tellurium ion bath)). The concentrations of  $\text{Pb}^{2+}$  and  $\text{HNO}_3$  were fixed at 0.05 and 1 M, respectively.

Prior to electrodeposition, cyclic voltammetry (CV) and linear sweep voltammetry (LSV) were performed to investigate the deposition mechanisms. Voltammograms were performed in a conventional three-electrode cell configuration with rotating disk electrode (RDE) (3 mm in diameter platinum disk embedded in a cylindrical Teflon holder) as a working electrode. Pt wire and  $\text{Ag}/\text{AgCl}$  (sat. KCl) were used as a counter and reference electrode, respectively. The temperature was kept at room temperature and the scan rate was fixed at 10 mV/s. The rotating rate of the RDE was varied from 100 to 5000 rpm to investigate the hydrodynamic effect.

After electroanalytical studies, the influence of the solution composition, deposition potential and temperature on deposition rate, film composition, crystallographic structure and their morphologies have been studied to determine optimum conditions to deposit high quality PbTe thin films. In the experiments, the working electrodes were evaporated gold thin film on silicon wafers and the counter electrode was a platinum-coated titanium stripe. The solutions were magnetically stirred at 300 rpm.

The film composition was determined by Atomic Absorption Spectroscopy (AAS, Perkin Elmer, Analyst 800). The film morphology and crystallographic structure were investigated by SEM (LEO 1550 VP FESEM) and X-ray diffraction method (Bruker D8 Advance Diffractometer with  $\text{Cu K}\alpha$  radiation).

## 3. Results and discussion

### 3.1. Electroanalytical studies of tellurium, lead and lead telluride electrodeposition

Fig. 1 shows cyclic voltammograms for tellurium (A), lead (B) and lead telluride (C) electrodeposition. Electrolyte compositions for tellurium, lead and lead telluride were 0.01 M

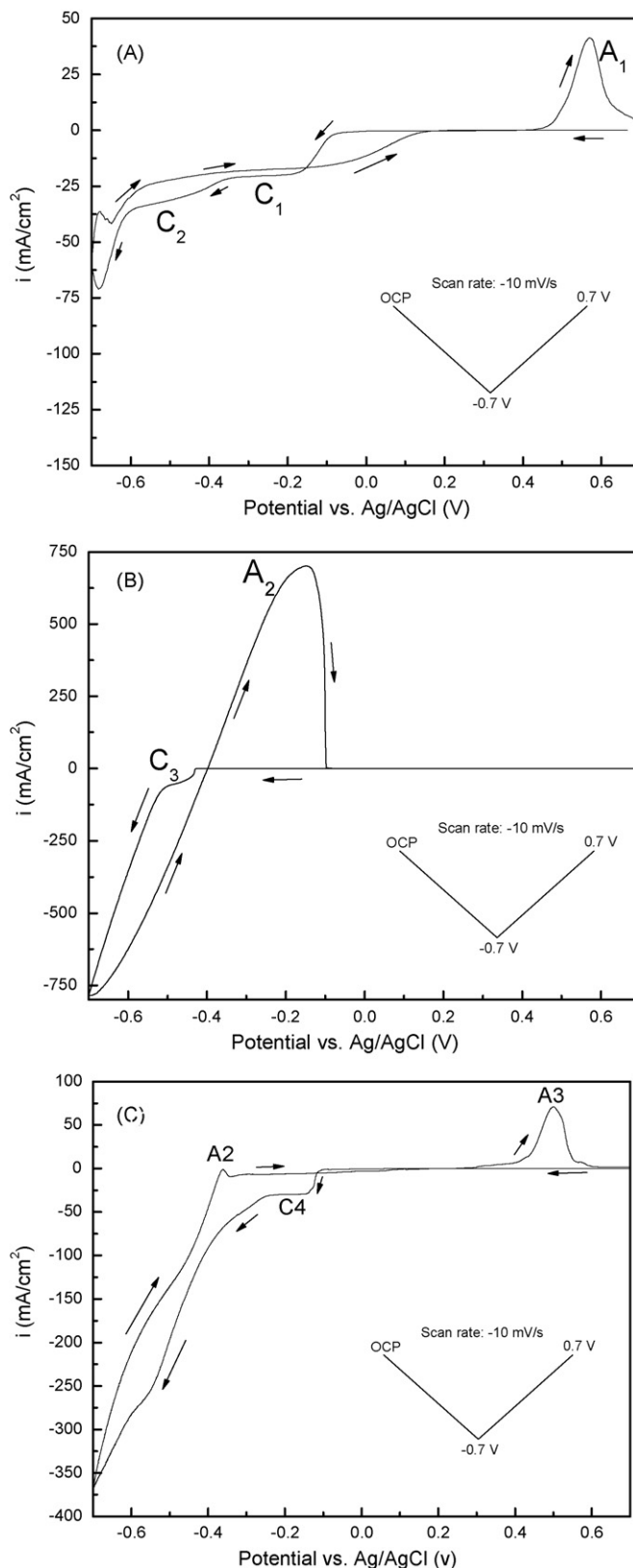
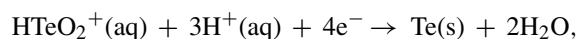


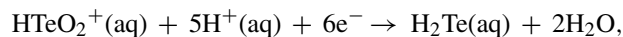
Fig. 1. Cyclic voltammograms for Te (A), Pb (B) and PbTe (C) electrodeposition from 10 mM  $\text{HTeO}_2^+$  + 1 M  $\text{HNO}_3$ , 0.05 M  $\text{Pb}^{2+}$  + 1 M  $\text{HNO}_3$  and 10 mM  $\text{HTeO}_2^+$  + 0.05 M  $\text{Pb}^{2+}$  + 1 M  $\text{HNO}_3$ , respectively. The potential scanning rate and rotating rate of RDE were fixed at 10 mV/s and 1000 rpm, respectively. Inside plot shows the potential profile applied.

$\text{HTeO}_2^+ + 1 \text{ M HNO}_3$ ,  $0.05 \text{ M Pb}^{2+} + 1 \text{ M HNO}_3$  and  $0.01 \text{ M HTeO}_2^+ + 0.05 \text{ M Pb}^{2+} + 1 \text{ M HNO}_3$ , respectively. The rotation rate of the RDE was fixed at 1000 rpm.

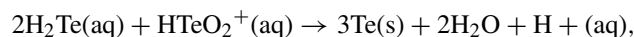
In tellurium electrodeposition, two reduction waves, labeled as  $C_1$  and  $C_2$ , respectively, were observed in the cathodic scan (Fig. 1A). The third reduction wave at  $\sim -0.68 \text{ V}$  was attributed to hydrogen evolution. The reduction reaction at  $C_1$  could be represented by Eq. (1) [17]. The deposit formed at  $C_1$  was identified as elemental Te by AAS and XRD. At  $C_2$ , a two-step reaction was proposed by others [18], which involves the electrochemical generation of  $\text{H}_2\text{Te}$  as an intermediate species (Eq. (2)) followed by chemical reduction to elemental Te (Eq. (3)). The overall process behaved as a four-electron reduction from  $\text{HTeO}_2^+$  to Te which was equivalent to Eq. (1). During the anodic scan, one oxidation peak was observed at  $\sim 0.57 \text{ V}$  (labeled as  $A_1$ ), which was caused by the dissolution of the Te electrodeposition.



$$E^\circ = +0.551 \text{ V versus NHE} \quad (1)$$



$$E^\circ = +0.121 \text{ V versus NHE} \quad (2)$$



$$\Delta G^\circ_f = -498.118 \text{ kJ/mol} \quad (3)$$

The hydrodynamic effect on the tellurium electrodeposition was investigated by varying the rotation rate from 100 to 5000 rpm (data not shown). The limiting current density at  $C_1$  has a linear relationship with the square root of the rotation rate ( $\omega^{1/2}$ ), which indicates that the electrodeposition of Te was controlled by the diffusion of  $\text{HTeO}_2^+$  to the electrode surface according to the Levich equation [19]. The diffusion coefficient for  $\text{HTeO}_2^+$  was determined to be  $6.8 \times 10^{-6} \text{ cm}^2/\text{s}$ , which agreed well with previously reported values [20].

Fig. 1B shows a cyclic voltammogram for Pb electrodeposition. One reduction wave (labeled as  $C_3$  starting at  $\sim -0.43 \text{ V}$ ) was observed during the cathodic scan. Analysis of the deposit at  $C_3$  by AAS identified the reduced material as elemental Pb. During the anodic scan, an oxidation peak (labeled as  $A_2$ ) was observed at  $-0.15 \text{ V}$ , which was caused by the stripping of the Pb deposit.

The cyclic voltammogram for PbTe electrodeposition is shown in Fig. 1C. During the cathodic scan, a limiting current (labeled as  $C_4$ ) was observed in the potential range of the limiting current for Te electrodeposition. The value of the former limiting current density was 1.46 times greater than the latter as shown in Fig. 2. The composition analyses of the deposits revealed Pb was co-deposited with Te in that potential range. This induced deposition of Pb on Te is called underpotential deposition (UPD), which has been reported in the electrodeposition of cadmium telluride [21]. PbTe electrodeposition can be described by a two-step mechanism whereby Te is first overpotentially deposited and then,  $\text{Pb}^{2+}$  ions react with Te atoms to form the PbTe compound. The overall process can be repre-

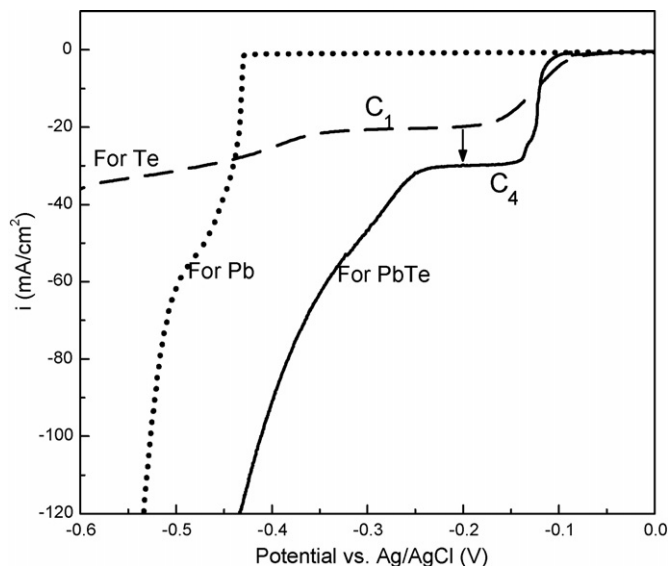
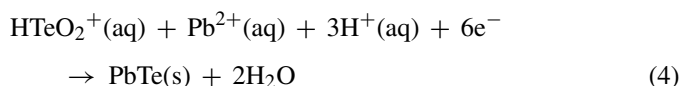


Fig. 2. Linear sweep voltammograms for Pb, Te and PbTe electrodepositions. The potential scanning rate and rotating rate of RDE were fixed at  $10 \text{ mV/s}$  and  $1000 \text{ rpm}$ , respectively.

sented by Eq. (4).



The activation energy for the UPD of Pb is from the free energy of PbTe formation,  $\Delta G^\circ_{f,\text{PbTe}} = -69.5 \text{ kJ/mol}$  [22], which shifts the potential of Pb electrodeposition to a more positive value by  $\Delta E = 0.36 \text{ V}$  according to  $\Delta E = \Delta G^\circ_{f,\text{PbTe}}/2F$  [17] where  $F$  is the Faraday constant.

During the anodic scan, two oxidation peaks appeared at  $-0.36 \text{ V}$  (labeled as  $A_2$ ) and  $+0.5 \text{ V}$  (labeled as  $A_3$ ), respectively. The oxidation peak  $A_2$  was due to the stripping of metallic Pb, but the area under  $A_2$  was much smaller than that observed

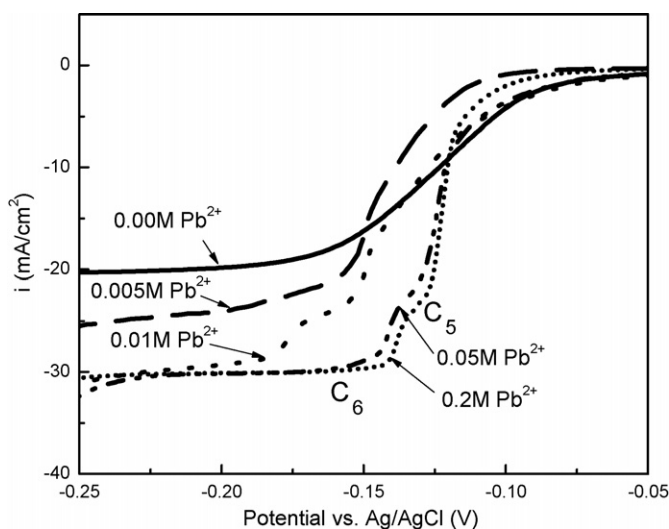


Fig. 3. Linear sweep voltammograms for PbTe electrodeposition from  $0.01 \text{ M HTeO}_2^+$  and  $X \text{ M Pb}^{2+}$  ( $X=0, 0.005, 0.01, 0.05$  and  $0.2$ ) in  $1 \text{ M HNO}_3$ . The potential scanning rate and rotating rate of RDE were fixed at  $10 \text{ mV/s}$  and  $1000 \text{ rpm}$ , respectively.

in the voltammetry for Pb electrodeposition (Fig. 1B), which is results from the formation of PbTe preventing the oxidation of Pb in PbTe. The oxidation peak A<sub>3</sub> is most likely attributed to the stripping of PbTe or elemental Te.

Similar to Te electrodeposition, hydrodynamic effects on PbTe electrodeposition were also studied by varying rotating rates ( $\omega$ ) from 100 to 5000 rpm (data not shown). The linear relationship between the limiting current density and  $\omega^{1/2}$  satisfies the Levich equation, meaning the electrodeposition was mass-transfer controlled. However, in this case, two electroactive species, HTeO<sub>2</sub><sup>+</sup> and Pb<sup>2+</sup>, were present in solution and either one or both components might dominate the electrodeposition rate. Therefore, LSVs were also carried out in solutions containing 0.01 M HTeO<sub>2</sub><sup>+</sup> with variable Pb<sup>2+</sup> concentration from 0 to 0.2 M (Fig. 3). As more Pb<sup>2+</sup> was progressively added to the solution, two cathodic waves (labeled as C<sub>5</sub> and C<sub>6</sub>, respectively) gradually developed. The first wave, C<sub>5</sub>, corresponded to

Te deposition and C<sub>6</sub> corresponded to PbTe deposition. Both waves showed give a progressive shift to more anodic potentials as the concentration of Pb<sup>2+</sup> increased because of the UPD of Pb on Te. The limiting current density at C<sub>6</sub> increased at lower Pb<sup>2+</sup> concentrations, simultaneously with the shifts of C<sub>5</sub> and C<sub>6</sub>, stabilizing above 0.01 M Pb<sup>2+</sup>. The result implied that the electrodeposition rate in the limiting current range was primarily controlled by the diffusion of HTeO<sub>2</sub><sup>+</sup> when Pb<sup>2+</sup> concentration was sufficiently high. Therefore, in the solution of 0.01 M HTeO<sub>2</sub><sup>+</sup>, 0.05 M Pb<sup>2+</sup> and 1 M HNO<sub>3</sub>, the limiting current density of PbTe electrodeposition can be calculated by Eq. (5) [23,24]:

$$i_{l, \text{PbTe}} = \frac{6FD[\text{HTeO}_2^+]}{\delta} \quad (5)$$

Similarly, the limiting current density of Te electrodeposition in 0.01 M HTeO<sub>2</sub><sup>+</sup> and 1 M HNO<sub>3</sub> is given by

$$i_{l, \text{Te}} = \frac{4FD[\text{HTeO}_2^+]}{\delta} \quad (6)$$

In Eqs. (5) and (6),  $D$  is the diffusion coefficient of HTeO<sub>2</sub><sup>+</sup> ions,  $F$  the Faraday constant and  $\delta$  is the thickness of the diffusion layer and [HTeO<sub>2</sub><sup>+</sup>] the concentration of HTeO<sub>2</sub><sup>+</sup>. Since [HTeO<sub>2</sub><sup>+</sup>] for Te and PbTe deposition was equal, the limiting current density was proportional to the number of reaction electrons involved, *i.e.*,  $i_{l, \text{PbTe}}/i_{l, \text{Te}} = 6/4 = 1.5$ . The limiting current density obtained from Fig. 2 was  $-20.34$  and  $-29.7$  mA/cm<sup>2</sup> respectively. The ratio ( $i_{l, \text{PbTe}}/i_{l, \text{Te}}$ ) obtained from our experiments was 1.46 and was found to generate a deposit composition of 52 at.% Te and 48 at.% Pb.

Temperature effects on the electrodeposition of PbTe were determined by varying the temperature from 24 to 60 °C (data not shown). The limiting current density was increased with the increase in temperature, which was mainly due to the increase of diffusivity. Since the limiting current density  $i_{\text{lim}}$  changed linearly with  $T^{2/3}$ , the diffusivity changed is displayed a nearly

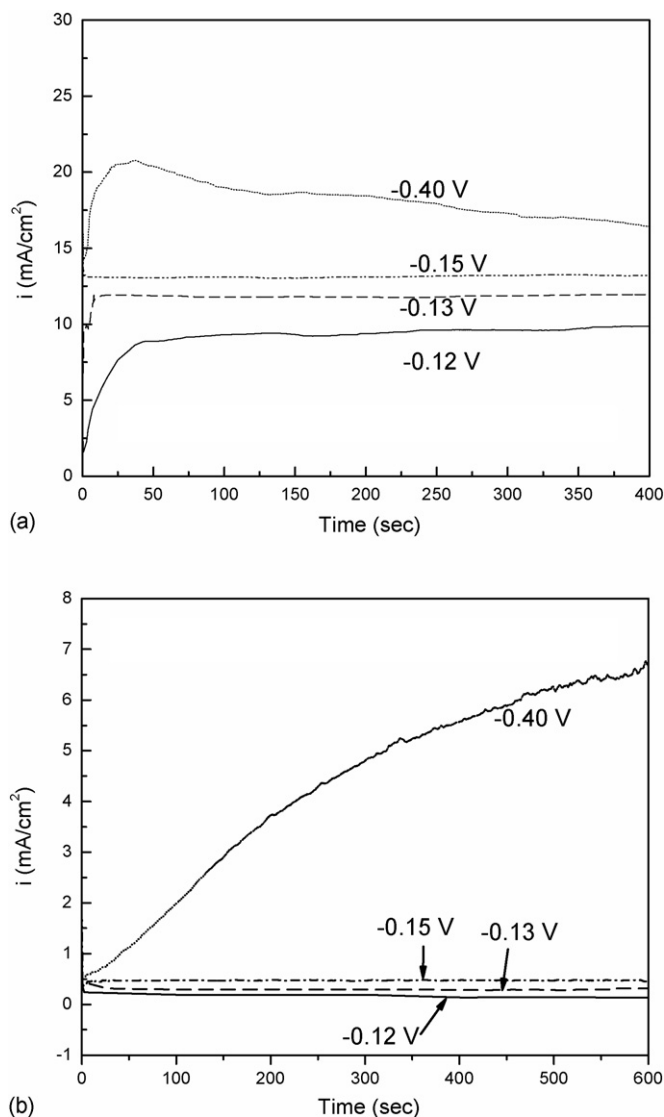


Fig. 4. Chronoamperograms of PbTe electrodeposition in: (a) 0.01 M HTeO<sub>2</sub><sup>+</sup> solution and (b) 0.0001 M HTeO<sub>2</sub><sup>+</sup> solution. Pb<sup>2+</sup> and HNO<sub>3</sub> concentration were fixed at 0.05 and 1 M, respectively.

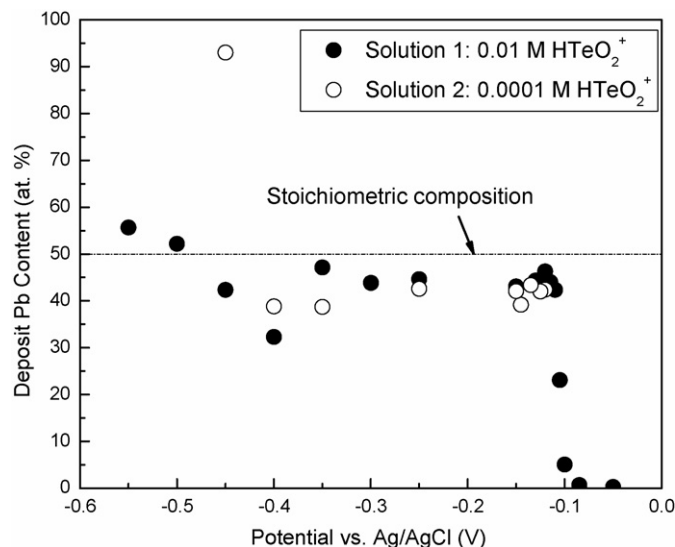


Fig. 5. Dependence of deposit Pb content on applied deposition potentials. The solution was magnetically stirred at 300 rpm. Temperature was fixed at 24 °C.

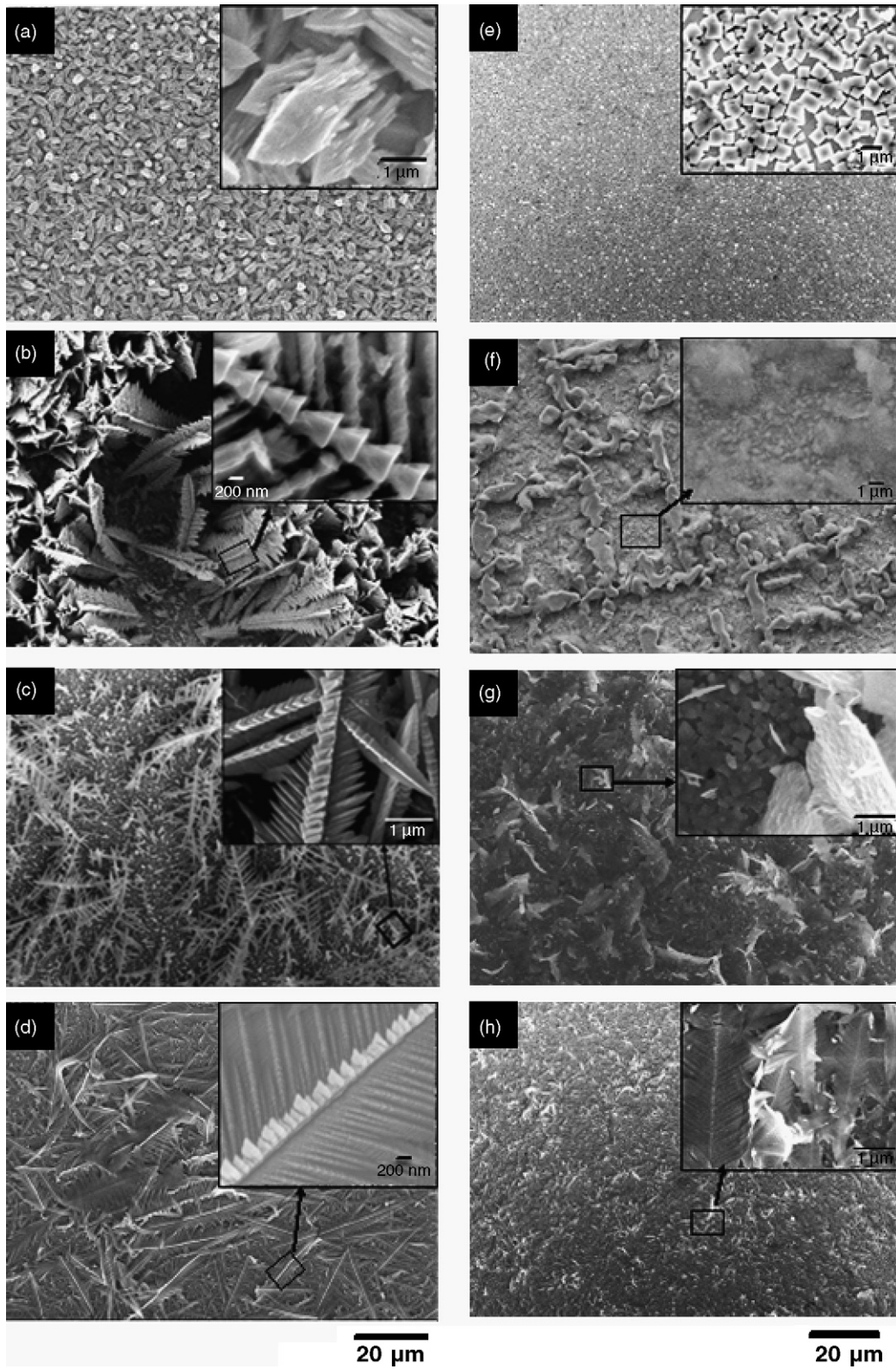


Fig. 6. SEM micrographs of PbTe films electrodeposited from 0.01 M  $\text{HTeO}_2^+$  solution at: (a) -0.12 V, (b) -0.13 V, (c) -0.15 V, (d) -0.40 V; and from 0.0001 M  $\text{HTeO}_2^+$  solution at (e) -0.12 V, (f) -0.13 V, (g) -0.15 V and (h) -0.40 V.

linear relationship with temperature, agreeing well with the Stokes–Einstein equation [25].

### 3.2. Electrodeposition of PbTe thin films

Based on the above electroanalytical studies, PbTe films were potentiostatically electrodeposited on gold-coated silicon wafers from 0.01 M  $\text{HTeO}_2^+$  solution (0.01 M  $\text{HTeO}_2^+$  + 0.05 M  $\text{Pb}^{2+}$  + 1 M  $\text{HNO}_3$ ) and 0.0001 M  $\text{HTeO}_2^+$  solution (0.0001 M  $\text{HTeO}_2^+$  + 0.05 M  $\text{Pb}^{2+}$  + 1 M  $\text{HNO}_3$ ). Fig. 4 shows the chronoamperograms of PbTe electrodeposition. As expected, the cathodic current density increased when the applied potential became more negative. The increase of initial cathodic current density when applied potential became more negative indicated that the nucleation rate increased for 0.01 M  $\text{HTeO}_2^+$  solution. As for 0.0001 M  $\text{HTeO}_2^+$  solution, the initial cathodic current density was independent of applied potential suggesting that the nucleation rates were almost the same at all the four potentials. Fig. 5 shows the film compositions obtained in 0.01 M  $\text{HTeO}_2^+$  and 0.0001 M  $\text{HTeO}_2^+$  solutions as a function of deposition potentials. In 0.01 M  $\text{HTeO}_2^+$  solution, the onset deposition potential for the UPD of Pb was around  $-0.1$  V, at which the Pb content increased abruptly from almost naught. Therefore, the potential of Pb UPD was  $\sim 0.33$  V more positive than the potential ( $\sim -0.43$  V) of independent Pb electrodeposition. The Pb potential shift is nearly the same as calculated from  $\Delta G^\circ_{\text{f,PbTe}}$  which is 0.36 V. In the mass-transfer controlled range (i.e.  $\sim -0.14$  to  $\sim -0.35$  V), the film composition remained almost constant at 54 at.% Te and 46 at.% Pb, which was very close to the composition predicted above by the ratio of the limiting current densities. At potentials more negative than  $-0.43$  V, metallic Pb was overpotentially deposited (OPD) leading to Pb-rich films. In 0.0001 M  $\text{HTeO}_2^+$  solution, the Pb contents obtained by UPD were not improved relative to those for 0.01 M  $\text{HTeO}_2^+$  solution. From  $\sim -0.43$  to  $\sim 0.50$  V, the films mainly consisted of metallic Pb. At more negative potentials than  $-0.50$  V, films could not be deposited. In both solutions, the PbTe films obtained by UPD were always slightly Te rich. The similar non-stoichiometry has also been observed in the electrodeposition of PbTe films from the alkaline solution at pH 9 [16].

Figs. 6 and 7 show the SEM micrographs and X-ray diffraction patterns of the films obtained at  $-0.12$ ,  $-0.13$ ,  $-0.15$  and  $-0.40$  V from the two solutions. The insets show the detailed microstructures of the squared regions. In 0.01 M  $\text{HTeO}_2^+$  solution, the film deposited at  $-0.12$  V was dense, uniform and silver-gray. According to the XRD pattern shown in Fig. 9a, the film had a preferred orientation in the  $[100]$  direction based on the difference in the standard (JCPDS, 38–1435) and experimental peak intensities. At  $-0.13$  V, the film growth was dendritic. The feather-like dendrites were perpendicular to the substrate with a highly preferred  $[211]$  orientation, exhibiting a well-defined crystallographic structure. The stem of the dendrite consisted of a string of pyramid crystals. At  $-0.15$  and  $-0.40$  V, XRD patterns revealed similar dendrites also in the preferred  $[211]$  direction. The contrasting reflections for 0.0001 M  $\text{HTeO}_2^+$ , shown in Fig. 9(b), indicate significant changes in the crystal structures. The film deposited at  $-0.12$  V consisted of

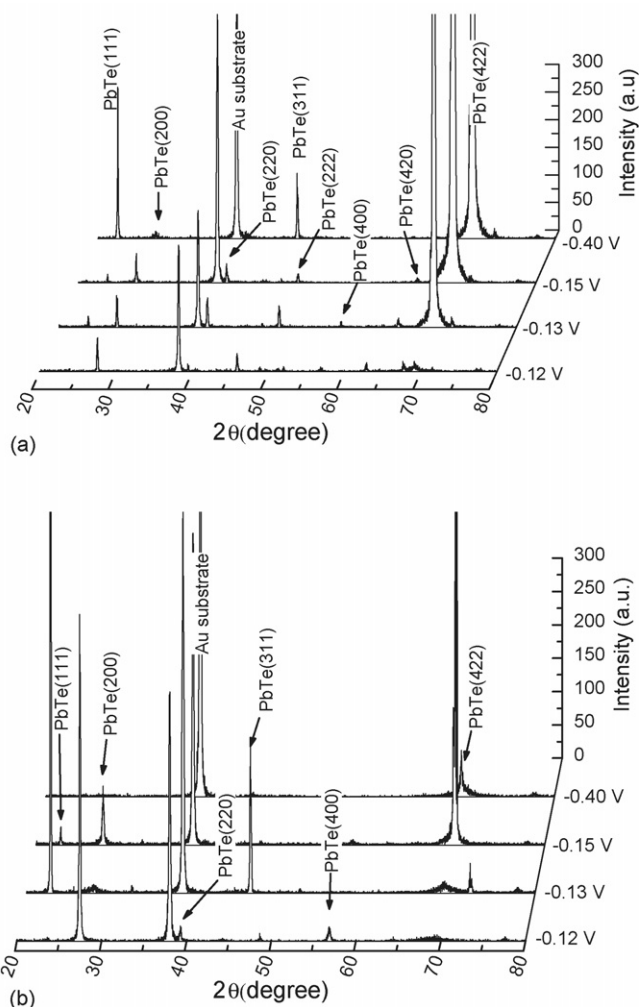


Fig. 7. XRD patterns of PbTe films electrodeposited from: (a) 0.01 M  $\text{HTeO}_2^+$  solution, and (b) 0.0001 M  $\text{HTeO}_2^+$  solution.

separate cubic crystals oriented along the  $[100]$  direction. The PbTe cubic crystals were not observed at  $-0.13$  V, and the  $(200)$  reflection became very weak as well. The film was preferentially oriented in the  $[111]$  direction. At  $-0.15$  V, some cubic crystals were observed again, which were probably responsible for the  $(200)$  reflection in the XRD pattern. Some dendrites were seen at this potential which looked brighter in the SEM image. These dendrites were suspected determinants of the strong  $(422)$  reflection observed in the XRD pattern. At  $-0.40$  V, feather-like dendrites were observed, which caused the  $(422)$  reflection. The fairly low intensity of the  $(422)$  reflection was probably a consequence of the low crystallinity of these dendrites.

To investigate the temperature effect on the film compositions, PbTe films were electrodeposited at various temperatures. The deposition potential was fixed at  $-0.12$  V. Fig. 8 shows the film composition as a function of the solution temperature. At room temperature, the electrodeposition at  $-0.12$  V was controlled by both the electron transfer rate and mass-transfer rate. Elevated temperatures pushed the balance into the mass-transfer controlled range, in which the deposition rate was dominated

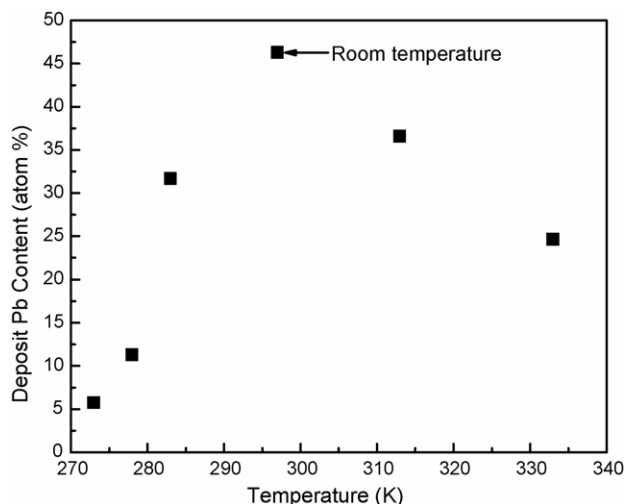


Fig. 8. PbTe film composition as a function of deposition temperature. Deposition potential was fixed at  $-0.12$  V vs. SCE.

by the diffusion of  $\text{HTeO}_2^+$ . As Fig. 8 indicates, the increase of  $\text{HTeO}_2^+$  diffusion rate with the temperature consequently reduced the Pb content in the deposit. Such a trend may also be applied to the stirring effect on the film composition obtained in the mass-transfer controlled range. Lowering the temperature, on the other hand, decreased the activation energy for the UPD of Pb and reduced the Pb content greatly.

#### 4. Conclusion

In summary, we have systematically investigated the electrodeposition of PbTe thin films from an acidic nitric baths. The reaction kinetics was initially studied with a rotating disk electrode to determine the mechanism of PbTe deposition. Based on electroanalytical studies, we concluded that PbTe was obtained by the underpotential deposition (UPD) of Pb atoms onto the overpotentially deposited Te atoms. The effect of deposition potential, solution composition and temperature on the film composition, crystallographic structure and texture were studied. The microstructure and preferred orientation of PbTe thin films changed greatly depending on the applied potential and electrolyte concentration. At  $-0.12$  V, the film was granular and oriented preferentially in the [100] direction. At potentials more negative than  $-0.15$  V, the film was dendritic and oriented preferentially in the [2 1 1] direction. A smooth, dense

and crystalline film with nearly stoichiometric composition was obtained at  $-0.12$  V from a solution containing  $0.01$  M  $\text{HTeO}_2^+$  +  $0.05$   $\text{Pb}^{2+}$  +  $1$  M  $\text{HNO}_3$ .

#### Acknowledgements

This work was supported by NASA Bio/Nano Program and Korea Institute of Machinery and Materials (KIMM).

#### References

- [1] H. Zogg, C. Maissen, J. Masek, T. Hoshino, S. Blunier, A.N. Tiwari, *Semi-cond. Sci. Technol.* 6 (1991) C36.
- [2] C. Boschetti, P.H.O. Rappi, A.Y. Ueta, I.N. Bandeira, *Infrared Phys.* 34 (1993) 281.
- [3] S.N. Chesnokov, D.E. Dolzhenko, I.I. Ivanchik, D.R. Khokhlov, *Infrared Phys. Technol.* 35 (1994) 23.
- [4] P.M. Nikolic, K. Radulovic, D. Vasiljevic-Radovic, et al., *J. Serb. Chem. Soc.* 67 (2002) 415.
- [5] Y.K. Yang, W.M. Li, L. Yu, et al., *Infrared Phys. Technol.* 38 (1997) 9.
- [6] A.S. Barros, E. Abramof, P.H.O. Rappi, *J. Appl. Phys.* 99 (2006) 024904.
- [7] F.J. DiSalvo, *Science* 285 (1999) 703.
- [8] G.D. Mahan, *Solid State Phys.* 51 (1998) 81.
- [9] T.C. Harman, D.L. Spears, M.P. Walsh, *J. Electron. Mater.* 28 (1999) L1.
- [10] K.F. Hsu, S. Loo, F. Guo, W. Chen, J.S. Dyck, C. Uher, T. Hogan, E.K. Polychroniadis, M.G. Kanatzidis, *Science* 303 (2004) 818.
- [11] H. Zogg, K. Alchalabi, D. Zimin, *Defence Sci. J.* 51 (2001) 53.
- [12] A. Jdanov, J. Pelleg, Z. Dashevsky, R. Shneck, *Mater. Sci. Eng. B-Solid State Mater. Adv. Technol.* 106 (2004) 89.
- [13] A.I. Fedorenko, A.G. Fedorov, A.Y. Sipatov, O.A. Mironov, *Thin Solid Films* 267 (1995) 134.
- [14] A. Jacquot, B. Lenoir, M.O. Boffoué, A. Dauscher, *Appl. Phys. A-Mater. Sci. Process.* 69 (1999) S613.
- [15] L. Beaunier, H. Cachet, R. Cortes, M. Froment, *J. Electroanal. Chem.* 532 (2002) 215.
- [16] H. Saloniemi, T. Kanninen, M. Ritala, M. Leskela, *Thin Solid Films* 326 (1998) 78.
- [17] M.P.R. Panicker, M. Knaster, F.A. Kroger, *J. Electrochem. Soc.* 125 (1978) 566.
- [18] M.S. Martín-González, A.L. Prieto, R. Gronsky, T. Sands, A.M. Stacya, *J. Electrochem. Soc.* 149 (2002) C546.
- [19] Southampton Electrochemistry Group, *Instrumental Methods in Electrochemistry*, Ellis Horwood Limited, Chichester, 1985.
- [20] T. Montiel-Santillán, O. Solorza, H. Sánchez, *J. Solid State Electrochem.* 6 (2002) 433.
- [21] D. Lincot, *Thin Solid Films* 487 (2005) 40.
- [22] CRC Handbook of Chemistry and Physics, CRC Press, Cleveland, 2002.
- [23] A.J. Bard, L.R. Faulkner, *Electrochemical Methods*, John Wiley and Sons, Inc., New York, 1980.
- [24] T. Ishizaki, T. Ohtomo, A. Fuwa, *J. Electrochem. Soc.* 151 (2004) C161.
- [25] R.H. Perry, D.W. Green, *Chemical Engineers' Handbook*, McGraw-Hill Inc., 1984.